Journal of Alloys and Compounds 765 (2018) 635–643

Contents lists available at ScienceDirect

Journal of Alloys and Compounds

journal homepage: http://www.elsevier.com/locate/jalcom

Kinetics and hydrogen storage performance of Li-Mg-N-H systems doped with Al and $AlCl_3$

Nina Senes [a], Luisa Fernández Albanesi [b], Sebastiano Garroni [c, d], Antonio Santoru [e], Claudio Pistidda [e], Gabriele Mulas [a], Stefano Enzo [a], Fabiana Gennari [b, *]

[a] Department of Chemistry and Pharmacy, University of Sassari and INSTM, Via Vienna 2, I-07100 Sassari, Italy
[b] Consejo Nacional de Investigaciones Científicas y Técnicas, CONICET - Centro Atómico Bariloche (CNEA), R8402AGP, S. C. de Bariloche, Río Negro, Argentina
[c] International Research Centre in Critical Raw Materials-ICCRAM, University of Burgos, Plaza Misael Bañuelos s/n, 09001 Burgos, Spain
[d] Advanced Materials, Nuclear Technology and Applied Bio/Nanotechnology, Consolidated Research Unit UIC-154. Castilla y Leon. Spain, University of Burgos, Hospital del Rey s/n, 09001 Burgos, Spain
[e] Institute of Materials Research, Materials Technology, Helmholtz-Zentrum Geesthacht GmbH, Max-Planck-Straße 1, 21502, Geesthacht, Germany

ARTICLE INFO

Article history:
Received 13 April 2018
Received in revised form
19 June 2018
Accepted 22 June 2018
Available online 23 June 2018

Keywords:
Hydrogen absorbing materials
Mechanochemical processing
Kinetics
Diffusion
Crystal structure

ABSTRACT

Recent investigations showed the formation of new amide-chloride phases between $LiNH_2$ and $AlCl_3$ after milling and/or heating under hydrogen pressure. These phases exhibited a key role in the improvement of the hydrogen storage properties of the $LiNH_2$-LiH composite. In the present work, we studied the effects of Al and $AlCl_3$ additives on the hydrogen storage behavior of the Li-Mg-N-H system. The dehydrogenation kinetics and the reaction pathway of Al and $AlCl_3$ modified $LiNH_2$-MgH_2 composite were investigated through a combination of kinetic measurements and structural analyses. During the first cycle, the addition of Al catalytically accelerates the hydrogen release at 200 °C. In the subsequent cycles, the formation of a new phase of unknown nature is probably responsible for both increased equilibrium hydrogen pressure and decreased dehydrogenation rate. In contrast, $AlCl_3$ additive reacts with $LiNH_2$-MgH_2 through the milling and continues during heating under hydrogen pressure. Addition of $AlCl_3$ leads to the formation of two cubic structures identified in the Li-Al-N-H-Cl system, which improves dehydrogenation rate by modifying the thermodynamic stability of the material. This study evidences positive effect of cation and/or anion substitution on hydrogen storage properties of the Li-Mg-N-H system.

1. Introduction

According to the Intergovernmental Panel on Climate Change (IPCC) report, to limit the global temperature increase to 1.5 °C, as stated in the last global climate accord in Paris, a larger emissions cut, in the range of 70–95%, would be required. In fact, despite the pledges to reduce the carbon foot prints in several developed countries, the greenhouse emissions are continuously increasing [1]. In the last years, in order to address this issue, the scientific community has put great effort into the implementation of zero-carbon energy sources [1,2].

In this scenario, the molecular form of hydrogen is an ideal energy carrier for a sustainable future due to its high energy density per unit weight (142 MJ/kg) and the fact that its product of combustion is only water [2]. However, for on-board applications, such as light-duty vehicle combined with Fuel Cell (FC) systems, the storage technology represents the major technical barrier to date. Storing hydrogen in solid-state materials, for example, has definite advantages over pressurized gaseous or cryogenically liquefied hydrogen due to the high volumetric hydrogen storage density and safety [2–5]. Nevertheless, intensive research is still necessary to develop a material able to ab/desorb hydrogen at temperatures below 80 °C with fast kinetics for more than 5000 cycles [5].

In the last decade, among the several classes of materials investigated for hydrogen storage purposes, the family represented by the amides (NH_2^-), alanates (AlH_4^-) and borohydrides (BH_4^-),

* Corresponding author. Consejo Nacional de Investigaciones Científicas y Técnicas (CONICET), Centro Atómico Bariloche (CNEA) and Instituto Balseiro (UNCu), Av. Bustillo 9500 R8402AGP Bariloche, Río Negro, Argentina.
E-mail addresses: senes.nina@gmail.com (N. Senes), lfernandez@cab.cnea.gov.ar (L. Fernández Albanesi), sgarroni@ubu.es (S. Garroni), antonio.santoru@hzg.de (A. Santoru), Claudio.Pistidda@hzg.de (C. Pistidda), mulas@uniss.it (G. Mulas), enzo@uniss.it (S. Enzo), gennari@cab.cnea.gov.ar (F. Gennari).

https://doi.org/10.1016/j.jallcom.2018.06.262
0925-8388/

attracted a lot of attention [6–8]. These systems are in fact characterized by a high hydrogen content, in most cases matching with the restricted targets fixed by the energy department of USA and Europe [8].

At first, the $2LiNH_2 + LiH$ system, with a maximum hydrogen storage capacity of 6.5 wt%, was indicated as a promising candidate due to its good thermodynamic characteristics ($\Delta H_r = 45$ kJ/molH_2) and reversibility under moderate pressures of 50 bar of hydrogen at 300 °C [9]. However, further studies showed that the desorption reaction is not concerted and it has serious limitations, such as the formation of NH_3 during the first dehydrogenation, and slow sorption kinetics under experimental conditions.

In order to deal with these issues, W. Luo et al. reported the destabilization of the $LiNH_2$ phase by a partial substitution of lithium with magnesium as showed in reaction (1) [10]:

$$2LiNH_{2(s)} + MgH_{2(s)} \rightarrow Li_2Mg(NH)_{2(s)} + 2H_{2(g)} \quad (1)$$

The formation of di-lithium magnesium imide, $Li_2Mg(NH)_2$, is achieved during the desorption path of reaction (1) with an important decrease of the desorption temperature. Surprisingly, when the ternary mixed imide is subjected to hydrogen pressure of 30 bar H_2 under temperatures slightly above 200 °C, the reaction proceeds with the formation of magnesium amide and lithium hydride as reported in reaction (2) [11]:

$$Li_2Mg(NH)_{2(s)} + 2H_{2(g)} \leftrightarrow Mg(NH_2)_{2(s)} + 2LiH_{(s)} \quad (2)$$

Recent studies demonstrated that the $Mg(NH_2)_2 + 2LiH$ composite is a prospective system for on-board hydrogen storage applications, with a theoretical enthalpy of 44 kJ/molH_2 and gravimetric capacity of 5.35 wt% H [11–14].

For these reasons, considerable effort has been put into improving the hydrogen storage properties of both composites exploring different strategies [15–35]. Very recently, Chen and coauthors reported that $LiBH_4$, added in stoichiometric amount, can considerably alter the thermodynamic and kinetic properties of the Mg-amide composite, leading to a full reversibility at temperatures lower than 100 °C [15]. In the past, a great deal of effort was devoted to the influence of metal hydrides, hydroxides and halides [19–33]. For example, KH and RbH, widely recognized as excellent additives for improving the sorption kinetics of the Li-Mg-N-H systems, can decrease the dehydrogenation temperature by 50–100 °C [20]. Improved hydrogen storage properties were also observed due to the addition of CsH and RbH [31,32]. Lithium halides can also enhance significantly the hydrogen storage properties of the $2LiNH_2 + MgH_2$ and $Mg(NH_2)_2 + 2LiH$ systems. Interestingly, the 0.2LiBr-doped sample reversibly stored 3.7 wt% H at about 185 °C [22]. Concerning the mechanism, it was demonstrated that LiBr reacts preferentially with $LiNH_2$, which was formed during the first desorption step, changing the reaction enthalpy of the whole system. To this regard, Anderson et al. reported that lithium/magnesium halides, reacting with $LiNH_2$, form new amide-halide phases with improved sorption properties and reduced ammonia gas evolution, when compared to the halide-free system [36]. Similar structures have also been observed in the $LiNH_2$-based systems when $AlCl_3$ is introduced as additive [37]. Recently, Gennari et al. proved the superior effect of $AlCl_3$ to destabilize the thermodynamic and kinetic properties of the $LiNH_2$ and $LiNH_2$-LiH systems [37–39]. Considering the remarkable effect of $AlCl_3$ on the above reported compounds, it is expected to achieve comparable performance by introducing it into $Mg(NH_2)_2 + 2LiH$ or $2LiNH_2 + MgH_2$ systems. However, by our knowledge, no data are reported on the Li-Mg-N-H systems doped by $AlCl_3$ additive.

Based on these considerations, we present a detailed investigation on the hydrogen sorption properties of the Li-Mg-N-H system doped with $AlCl_3$ and Al. The results achieved confirm the benefit of $AlCl_3$ and Al additives on the kinetics of dehydrogenation of the Li-Mg-N-H system. However, the cyclability of each modified composite was affected by the formation of new Al-based phases. A plausible reaction pathway for hydrogen release/uptake process of $AlCl_3$ doped Li-Mg-N-H system is here proposed.

2. Experimental methods

2.1. Preparation of aluminum doped Li- Mg-N-H samples

Commercial $LiNH_2$ (Aldrich, purity 95%), MgH_2 (Aldrich, 98%), Al (Aldrich 99.99%) and $AlCl_3$ (Merck, 98%) were used as starting materials.

According to a previous work [17], the preparation of the $Mg(NH_2)_2 + 2LiH$-based systems were carried out by a prolonged mechanical milling of the $LiNH_2$ and MgH_2 reagents in a molar ratio 2:1. The mixture was ball milled for 27 h under 0.1 MPa argon at 500 rpm using a planetary mill (Fritsch Pulverisette 6) with a ball to powder ratio of 40:1 [17]. The preparation of the Al- and $AlCl_3$-doped samples was performed by the mechanical treatment for 5 h of the $2LiNH_2 + MgH_2 + 0.09Al$ and $2LiNH_2 + MgH_2 + 0.09AlCl_3$ mixtures. Before introducing the dopants, the $2LiNH_2 + MgH_2$ powders were pre-milled for 22 h.

The starting reagents $LiNH_2$ and MgH_2 (2:1) were also ball milled without additives for 27 h.

All samples were handled in an argon-filled MBraun Unilab glove box, with oxygen and moisture levels lower than 1 ppm.

2.2. Characterization methods of the composites

Structural information of as-prepared and as-treated samples was obtained by X-ray powder diffraction (XRPD, PANalytical Empyrean, Cu Kα radiation, graphite monochromator) and Fourier-transform infrared spectroscopy (FTIR, Perkin Elmer Spectrum 400) analyses. To prevent oxidation during XRPD data collection, the samples were sealed under argon atmosphere using an air-tight sample holder. Qualitative and quantitative analysis of the XRPD patterns were performed by Rietveld refinement using MAUD software [40].

For FTIR spectroscopy measurements, pressed pellets were prepared under purified argon atmosphere by grinding of the samples with dry KBr. Solid state FTIR spectra were measured in the range of 4000–1000 cm^{-1} using a specially-designed cell closed in the glove box. The gases released during dehydrogenation at different temperatures were analyzed using a degassed quartz optical cell with KBr windows.

The mass change of as-milled and as-treated samples was measured using thermogravimetric equipment (TG-HP50, TA Instruments) under helium gas flow at a heating rate of 5 °C/min. Samples of about 5–7 mg were loaded into aluminum capsules closed in the glove box and transferred under inert atmosphere.

Hydrogen volumetric measurements were performed on an in-house made Sieverts' system, coupled with a mass flow controller. Each sample was transferred in the glove box into a stainless reactor which was connected to the Sieverts' device. The whole system was evacuated prior to measurement and purged several times with hydrogen gas. For isothermal measurements, the sample was heated up to 200 °C under hydrogen pressure (6.0 MPa), kept at this temperature for 0.5 h before measuring the hydrogen desorption (under 0.05 MPa). Re-hydrogenation measurements were performed at 200 °C at a constant hydrogen pressure of 6.0 MPa. In order to perform PCI measurements, each sample was heated up to 200 °C under 6.0 MPa of hydrogen for 0.5 h before

measuring the first dehydrogenation PCI curve. The hydrogen contents were expressed as wt% with respect to the total mass of each mixture.

3. Results and discussion

3.1. Dehydrogenation properties of the Al and $AlCl_3$-doped $2LiNH_2 + MgH_2$samples

In order to assess the effects of aluminum additives on the hydrogen storage properties of the Li-Mg-N-H system, the hydrogen desorption and decomposition behaviors were determined by volumetric and thermogravimetric analyses, respectively. The results are showed in Figs. 1 and 2. For comparison purposes, the corresponding curves of the pristine ball-milled system (black circles), are also included.

It can be seen from Fig. 1A that the as-milled materials exhibited a two-step dehydrogenation process: the first step, between 150 and 200 °C, and the second one, between 200 and 400 °C. For the $AlCl_3$-doped system the decomposition profile was identical to that of the undoped sample up to 200 °C, which suggests that $AlCl_3$ did not influence the decomposition behavior of this mixture. In the case of the Al addition, the decomposition temperature decreased, which hints toward a possible participation of Al in the first dehydrogenation cycle. Mass loss achieved upon heating to 200 °C was 3 wt% H for the Al-doped sample, while for the undoped and $AlCl_3$-doped samples it was around 2 wt% H. Increasing the temperature up to 400 °C induces a mass loss exceeding 5.5 wt% H (theoretical wt% loss from reaction 1), mainly ascribable to the release of minor amounts of ammonia by-product. In fact, FTIR gas analysis showed presence of NH_3 during dehydrogenation at temperatures higher than 300 °C. Moreover, the ammonia release increased with temperature.

After thermal treatment at 200 °C under 6.0 MPa of hydrogen, the two-step dehydrogenation process shifted to a higher temperature, with the first step taking place between 150 and 225 °C, and the second one between 225 and 400 °C (Fig. 1B). Both doped composites display improved dehydrogenation rates at temperatures lower than 200 °C. It is noted that a change in the decomposition behavior occurs at 200–225 °C, and that ammonia emission gains relevance at higher temperatures due to the thermal decomposition of $LiNH_2$ upon heating. Due to NH_3 emission, the mass loss measured was higher than the theoretical hydrogen capacity for each sample (Fig. 1A and B). For these reasons, additional kinetics and structural studies were performed at 200 °C.

All as-milled samples underwent heating under 6.0 MPa of hydrogen up to 200 °C for 0.5 h. After this procedure, isothermal dehydrogenation curves at 200 °C were acquired and displayed in Fig. 2. For simplicity, the three thermally treated systems are indicated as LM, LMAl and LMAlCl. It can be seen that the first dehydrogenation cycle of the Al-doped sample was accelerated with respect to that without the additive, both releasing a total hydrogen content of 5.0 wt%. Considering the slope of hydrogen released as a function of time (Fig. 2) between 0.02 wt% and 0.25 wt %, a dehydrogenation rate of 0.22 ± 0.05 wt% min^{-1} was obtained for the LM sample during the first cycle, in comparison to 0.42 ± 0.05 wt% min^{-1} for the LMAl sample. This improvement in dehydrogenation rate was not observed during the second cycle, where Al-doped and undoped samples exhibited a similar initial rate with a reduction in the hydrogen storage capacity of the Al-doped sample. Additional cycling of the Al-doped sample showed a similar dehydrogenation behavior to the second cycle. On the other hand, dehydrogenation kinetics of the $AlCl_3$-doped sample was also faster than that of the LM. In fact, a dehydrogenation rate of 0.66 ± 0.05 wt% min^{-1} was obtained for the LMAlCl sample during the first cycle, in comparison to 0.22 ± 0.05 wt% min^{-1} for the LM sample. Again, a strong reduction of the amount of hydrogen released was observed in the second cycle for the $AlCl_3$-doped system. It can be concluded that the dehydrogenation rate was about two and about three times faster due to the addition of Al and $AlCl_3$, respectively.

Apparently, some changes in the Al- and $AlCl_3$-doped samples occurred during hydrogen cycling as a consequence of the interaction between the reactants, which could partially change phases present in the system and, consequently, the kinetics and/or equilibrium hydrogen pressure at 200 °C. In the following part, structural modifications in the samples doped by different aluminum additives will be studied and analyzed.

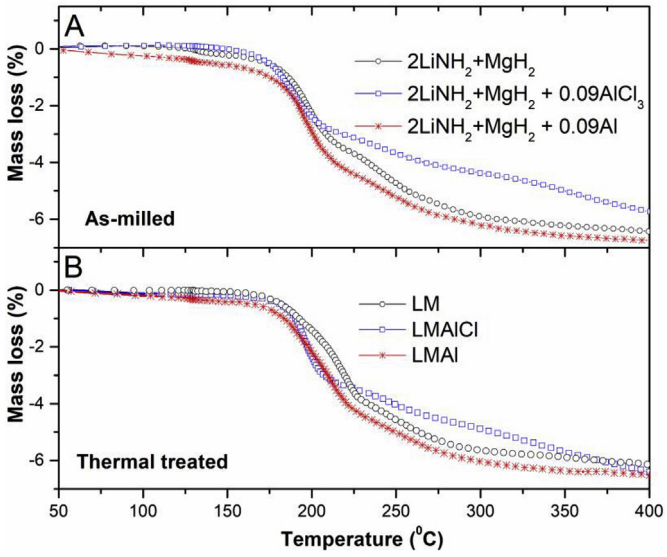

Fig. 1. TG curves of Al-doped and $AlCl_3$-doped samples obtained after: A) milling and B) thermal treatment. The as-milled and treated $2LiNH_2$-MgH_2 samples are showed as reference.

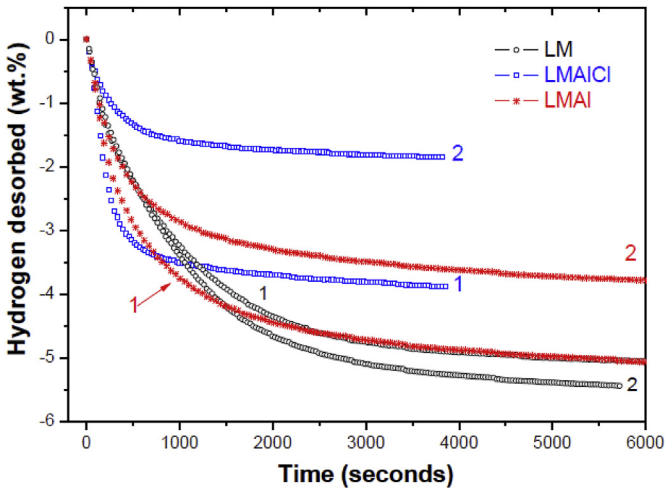

Fig. 2. Isothermal hydrogen desorption at 200 °C of Al-doped (LMAl) and $AlCl_3$-doped (LMAlCl) samples. The numbers 1 and 2 indicate 1st and 2nd cycle, respectively. Sample $2LiNH_2 + MgH_2$ milled for 27 h and thermal treated (LM) is showed as reference.

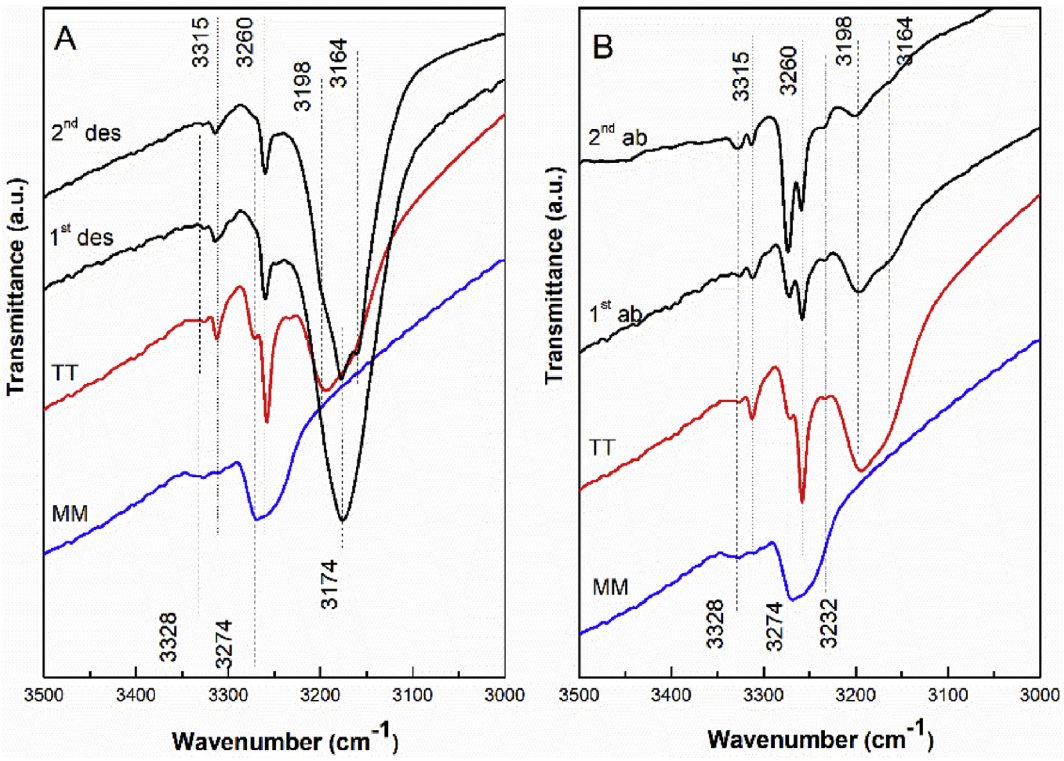

Fig. 3. FTIR spectra of the Al-doped sample (LMAl) after A) first and second desorption at 200 °C; B) first and second absorption at 200 °C. For comparison, the spectra of Al doped-sample after mechanical milling and thermal treatment under 6.0 MPa of hydrogen at 200 °C are also included.

3.2. Structural modifications of the Al- and $AlCl_3$-doped $2LiNH_2 + MgH_2$samples during hydrogen sorption

In order to clarify the structural changes in samples during hydrogen sorption and the effect of aluminum additives, several samples were collected at different stages for FTIR (Figs. 3 and 5) and XRPD (Figs. 4 and 6) analyses.

In the case of the sample modified by Al addition, the FTIR spectrum of as-milled sample exhibited the characteristic N-H vibrations attributed to the amide ions in $Mg(NH_2)_2$ at 3328 and 3274 cm^{-1}, demonstrating that during the milling, $Mg(NH_2)_2$ was formed (Fig. 3A). After thermal treatment under 6.0 MPa of hydrogen at 200 °C, in addition to the $Mg(NH_2)_2$ phase, the characteristic N-H vibration doublet of $LiNH_2$ at 3315 and 3260 cm^{-1} was detected. Simultaneously, bands at 3198 and 3164 cm^{-1} correlated with the formation of $Li_2Mg_2(NH)_3$ as a consequence of partial decomposition of $Mg(NH_2)_2$. The XRPD diffraction analysis confirms the presence of crystalline $Mg(NH_2)_2$ (70 wt%), in the

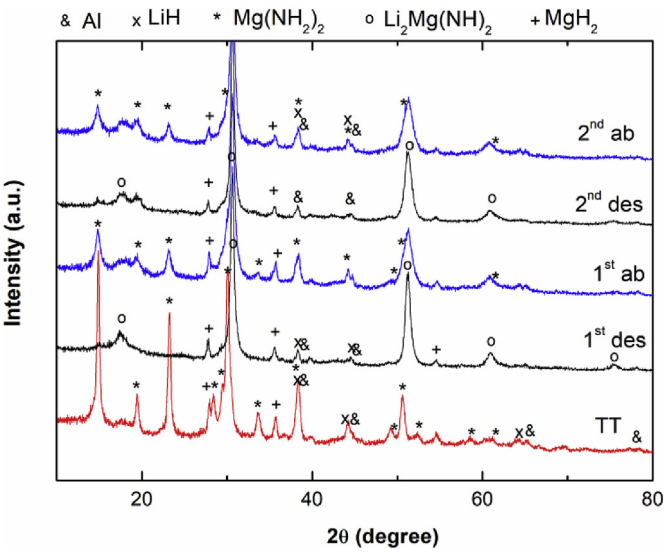

Fig. 4. XRPD patterns of the Al-doped sample (LMAl) after thermal treatment (TT), first and second cycles of hydrogen sorption at 200 °C (1st des, 1st ab; 2nd des, 2nd ab).

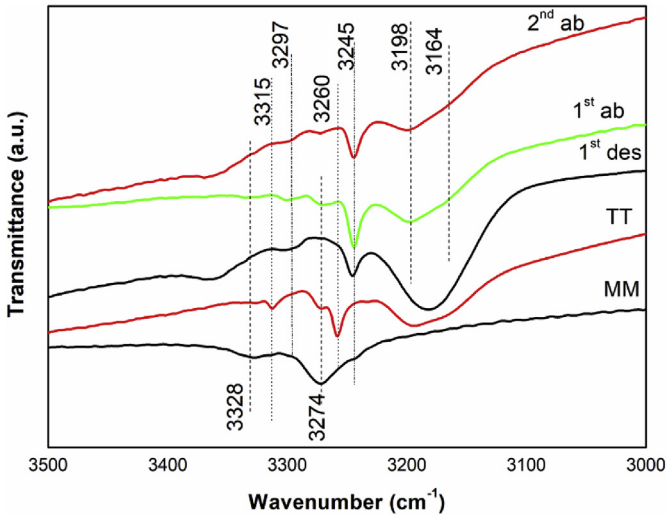

Fig. 5. FTIR spectra of the $AlCl_3$-doped sample, LMAlCl, after first hydrogen desorption cycle (1st des) and first and second hydrogen absorption cycles (1st and 2nd ab) at 200 °C. For comparison, the spectra of Al-doped sample after mechanical milling (MM) and thermal treatment (TT) under 6.0 MPa of hydrogen at 200 °C are also included.

hydrogen-treated sample (Fig. 4), and the characteristic diffraction peaks of LiH (25 wt%), Al (2 wt%), and unreacted MgH_2 (3 wt%) and $LiNH_2$ (<1 wt%). No diffraction peaks of $Li_2Mg_2(NH)_3$ were detected probably due to the formation of minor amounts of this phase, or with a very small crystallite size. After the first dehydrogenation, N-H vibrations related with $Mg(NH_2)_2$ disappeared, and the band at 3174 cm^{-1}, characteristic of the $Li_2Mg(NH)_2$, was clearly identified (Fig. 3A). This result and the XRPD pattern (Fig. 4) confirm the complete conversion of $Mg(NH_2)_2$ into cubic $Li_2Mg(NH)_2$ (96 wt%) during the first hydrogen desorption. At this stage, crystalline Al (3 wt%), LiH (<1 wt%) and MgH_2 (<1 wt%) phases were identified. The reversible hydrogen absorption-desorption cycling was just partial: the bands associated with $LiNH_2$ and $Li_2Mg(NH)_2$ remained in both dehydrogenated and hydrogenated state (Fig. 3A and B, respectively), as it was also confirmed from X-ray diffraction (Fig. 4). The quantitative Rietveld analysis concluded on the following composition: $Mg(NH_2)_2$ (38 wt%), LiH (12 wt%), Al (2 wt %), MgH_2 (2 wt%), $Li_2Mg(NH)_2$ (46 wt%), and $LiNH_2$ (<1 wt%). Moreover, a new band was detected at 3232 cm^{-1} in the hydrogenated state and its intensity increased with cycling (Fig. 3B). These findings suggest that a new species was possibly generated during successive hydrogen ab/de-sorption at 200 °C, which could not be assigned to any known reported phase. Recently, a new intermediate $Li_{4-x}Al_x(NH)_{2-2x}N_{2x}$ was identified during an interaction between Li_2NH and Al, which preceded the formation of Li_3AlN_2. However, its N-H vibration was blue-shifted (ranging from 3220 to 3120 cm^{-1}) compared with our result (3232 cm^{-1}) [41]. Moreover, $LiAl(NH)_2$ was formed during the decomposition of Li_3AlH_6-doped $Mg(NH_2)_2$-LiH sample [42], but its N-H position was also blue-shifted. Additional studies are required to clarify the nature of this interaction.

In the case of $AlCl_3$-doped system, Fig. 5 shows that after ball milling, the $AlCl_3$-doped sample consisted of $Mg(NH_2)_2$, as it can be inferred by the stretching bands at 3328 and 3274 cm^{-1} positions. After the thermal treatment, the bands from $Mg(NH_2)_2$ decrease, while those related with $Li_2Mg(NH)_2$ appear, suggesting a partial reaction of $Mg(NH_2)_2$. Simultaneously, peaks at 3315 and 3260 cm^{-1}, characteristic of $LiNH_2$, are identified. These two spectra are similar to those obtained for Al-doped samples (Fig. 3). However, the XRPD pattern obtained for the $AlCl_3$-doped sample after the thermal treatment under hydrogen reveals structural changes (Fig. 6). Although a significant amount of LiH phase is present (28 wt%), $Mg(NH_2)_2$ was not clearly detected by XPRD either due to the detection limit (>3 wt%), or due to its probable amorphous nature. Interestingly, two new sets of diffraction associated with the formation of two different cubic structures are visible [38]. One of these cubic compounds (Space Group $I2_13$), with a cell parameter of $a = 10.477$ Å, was previously associated with the reaction between $LiNH_2$ and $AlCl_3$ during heating, reaction which induces the formation of a Li-Al-N-H-Cl phase with stoichiometry $Li_3Al_{3x}(NH_2)_3Cl_{9x}$ [38]. The second sequence of peaks, indexed with a *Fm*-3*m* space group and with a cell parameter of $a = 5.152$ Å, was previously observed as a direct interaction of $AlCl_3$ and $LiNH_2$ during the ball milling of the product (*Fm*-3*m*, a = 5.231 Å, referred as $LiAl_x(NH_2)Cl_{3x}$) or upon the dehydrogenation of Li-Al-N-H-Cl phase in the presence of LiH (*Fm*-3*m*, a = 5.232–5.172 Å) [38]. These phases abundances are 21 and 42 wt% in the thermal-treated mixture. Finally, 8 wt% of MgH_2 is also found in the system.

The successive dehydrogenation leads to the formation of the cubic $Li_2Mg(NH)_2$ ($a = 5.022$ Å) as it can be inferred from XRPD pattern (Figs. 6 and 7), and the disappearance of LiH. Furthermore, an imide phase with $a = 5.159$ Å is also identified in the pattern. Similar cell parameters and peaks sequence have been found in the imide product upon the decomposition of the $3LiNH_2 + 1/3\ MgCl_2$ system, reported by Anderson et al. [36], and in the

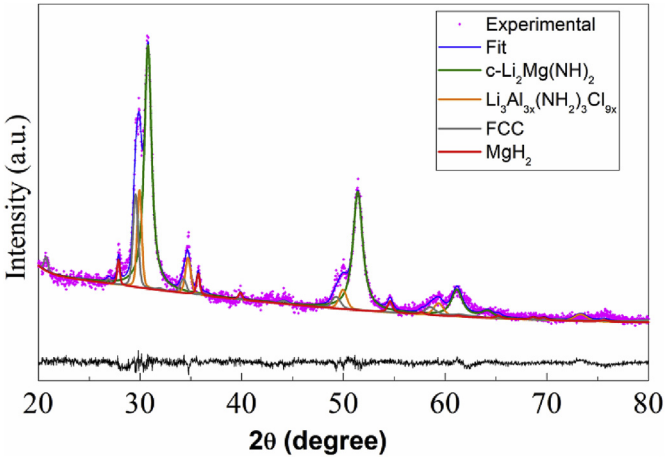

Fig. 7. XRPD pattern and the Rietveld analysis of the $AlCl_3$-doped sample, LMAlCl, after first hydrogen desorption cycle (1st des) at 200 °C.

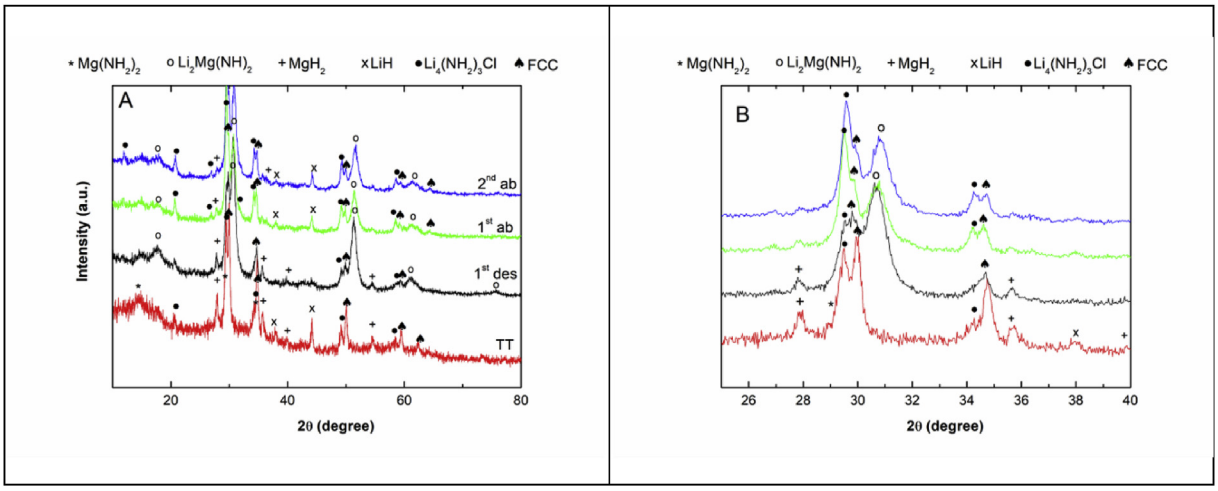

Fig. 6. XRPD patterns of the $AlCl_3$-doped sample, LMAlCl, after thermal treatment under 6.0 MPa of hydrogen (TT), first hydrogen desorption cycle (1st des) and second hydrogen absorption cycle (2nd ab), at 200 °C. In panel B, detail in the angular range 2Θ = 25–40 is given.

dehydrogenation of the $LiNH_2$-0.11$AlCl_3$ system [38]. The latter was indexed as a FCC-like sequence with a cell parameter between 5.232 and 5.172 Å.

FTIR confirms the presence of $Li_2Mg(NH)_2$ as well as the Li-Al-N-H-Cl phase. Consecutive hydrogen absorption-desorption cycles induce the progressive increase of the Li-Al-N-H-Cl phase by consumption of $LiNH_2$, as it was demonstrated by the absence of the bands at 3315 and 3260 cm^{-1}, and the corresponding XRPD pattern reported in Fig. 6.

3.3. Thermodynamic studies of Al- and $AlCl_3$-doped samples

Considering that the addition of Al and $AlCl_3$ to $2LiNH_2 + MgH_2$ modifies the dehydrogenation kinetics, it is of relevance to evaluate the thermodynamic stability of each composite. The pressure composition isotherms (PCIs) of the doped $2LiNH_2 + MgH_2$ samples were obtained after thermal treatment of as-milled samples at 200 °C with 6.0 MPa of hydrogen pressure. Typical hydrogen desorption isotherms are presented in Fig. 8. The first dehydrogenation PCI for the Al-doped sample displays a flat plateau at an equilibrium pressure slightly inferior to that of the undoped $2LiNH_2 + MgH_2$ sample (1.38 and 1.48 MPa, respectively). However, in the second dehydrogenation cycle, the hydrogen equilibrium pressure increases, showing a sloped plateau with an average equilibrium pressure higher than 2.0 MPa. This is additional evidence that a modification in the nature of the Al-doped sample happened after the first hydrogen desorption cycle. In contrast, the equilibrium pressure of the first dehydrogenation of $AlCl_3$-doped sample was about 1.7 MPa, which is a higher value than the one of the undoped material. This is an indication that the $2LiNH_2 + MgH_2 + 0.09AlCl_3$ composite constituted a destabilized system and the modifications in the composite took place before the first dehydrogenation. Therefore, both additives induced a destabilization of the $2LiNH_2 + MgH_2$ sample after interactions between the Al compounds and the reactants.

3.4. Kinetic investigations

To gain quantitative information on the kinetic constants involved in the hydrogen sorption of the Al- and $AlCl_3$-doped samples, the isothermal kinetic curves were fitted by analytical equations based on different solid-state reaction models, extensively discussed in previous manuscripts and summarized in Table 1 [43–46].

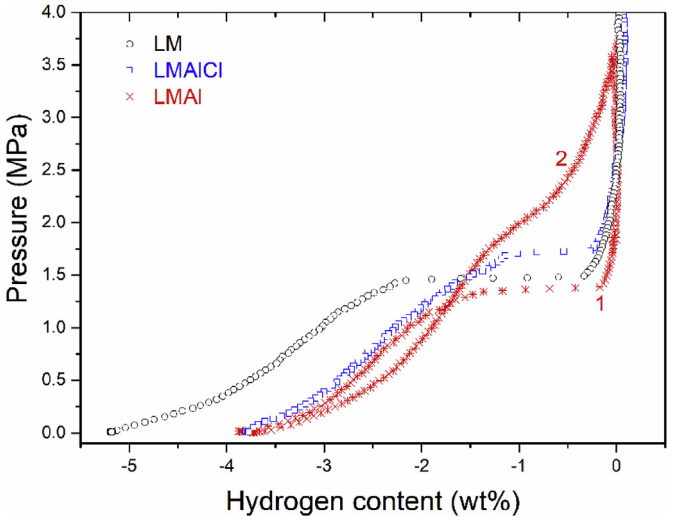

Fig. 8. Pressure composition isotherms of desorption at 200 °C for Al-doped and $AlCl_3$-doped $2LiNH_2 + MgH_2$ sample. The numbers 1 and 2 indicate the number of cycle.

Two main models, the diffusion controlled (D) and the phase-boundary controlled (R), describe the experimental kinetic curves of the doped and undoped systems. In addition, the empirical model F1 was also tested. In the first model, the diffusion is the rate-limiting step, while in the shrinking core model, the chemical reaction at the phase boundary controls the rate. By applying the equations in Table 1 to the experimental curves (Fig. 2), the best linearity obtained with respect to the reaction time allows to distinguish between the most appropriate models used for estimating the kinetic rate constant.

The results reported in Fig. 9, suggest that the dehydrogenation performance of the doped and undoped systems correspond more closely to the diffusion-controlled models (D), indicating that diffusion controls the rate of the reaction. However, it is not possible to fully discriminate between D3 and D4, although the best linear fit is obtained for the second kinetic model. The same approach was also applied to the second desorption cycle for all the systems, confirming the diffusion-controlled rate of the reaction. The values for each kinetic rate constant are tabulated in Table 2.

From the results tabulated in Table 2, it is possible to realize that system doped with $AlCl_3$ shows the highest kinetic rate ($4.52 * 10^{-5}$ s^{-1}), followed by the Al-doped and undoped systems. However, this trend cannot be confirmed for the second desorption steps where a significant decrease in the kinetic rates for both doped systems is observed, reaching values inferior to those of the undoped mixture.

3.5. Reaction pathway for hydrogen release from Al- and $AlCl_3$-doped samples

The structural investigations and the thermodynamic and kinetic studies of the doped composites provided relevant information about the intermediate and final products at different stages of synthesis and/or hydrogen cycling. The $2LiNH_2 + MgH_2$ mixture was first ball milled for 22 h to favor the formation of $Mg(NH_2)_2$ via metathesis reaction [17]:

$$2LiNH_{2(s)} + MgH_{2(s)} \text{—} \textit{ball milling} \rightarrow Mg(NH_2)_{2(s)} + 2LiH_{(s)} \quad (3)$$

No clear reaction of $Mg(NH_2)_2$ with Al occurred during extra milling for 5 h, while it is quite evident between $AlCl_3$ and metal amide phases. For the Al-doped $Mg(NH_2)_2 + 2LiH$ composite, the thermal treatment at 200 °C under 6.0 MPa of hydrogen did not induce detectable structural modifications. After the first dehydrogenation, the XRPD and FTIR studies showed that $Mg(NH_2)_2$ transformed into $Li_2Mg(NH)_2$ by the well-known two-step reaction [47]:

Table 1
List of the kinetic models and the rate equations used for fitting the isothermal desorption experiments. α = reacted fraction, k = kinetic rate constant, t = reaction time (s).

Reaction Model	Code	Equation
One-dimensional Diffusion	D1	$\alpha^2 = kt$
Two-dimensional Diffusion	D2	$(1-\alpha)\ln(1-\alpha)+\alpha = kt$
Three-Dimensional Diffusion (Jander)	D3	$\left(1-(1-\alpha)^{\frac{1}{3}}\right)^2 = kt$
Three-Dimensional Diffusion (Ginstling and Brounshtein)	D4	$\left(1-\frac{2\alpha}{3}\right)-(1-\alpha)^{2/3} = kt$
First-order kinetic	F1	$-\ln(1-\alpha) = kt$
Two-dimensional growth phase boundary	R2	$1-(1-\alpha)^{\frac{1}{2}} = kt$
Three-dimensional growth phase boundary	R3	$1-(1-\alpha)^{\frac{1}{3}} = kt$

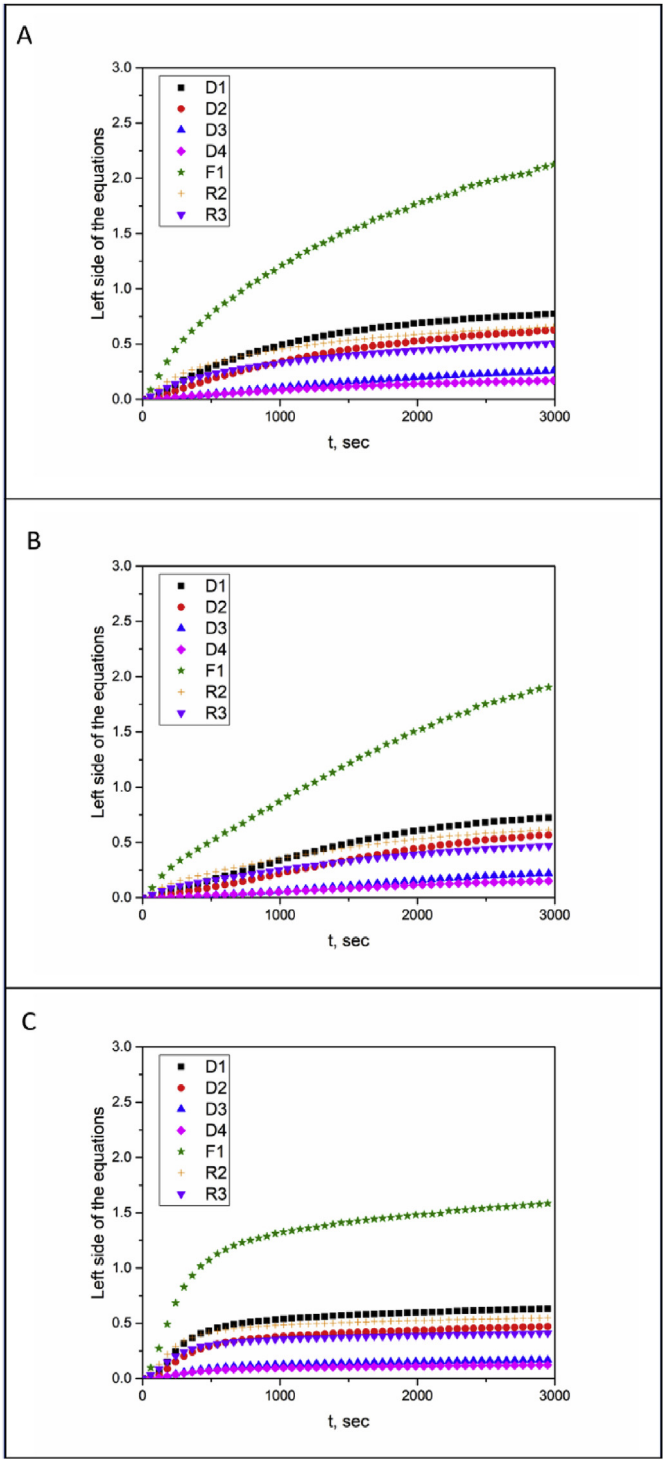

Fig. 9. Plot of different kinetic equations with respect to reaction time, applied to the 1st desorption step, operated at 200 °C, for the systems LM (A), LMAl (B) and LMAlCl (C).

$$2Mg(NH_2)_2 + 3LiH \rightarrow Li_2Mg_2(NH)_3 + LiNH_2 + 3H_2 \quad (4)$$

$$Li_2Mg_2(NH)_3 + LiNH_2 + LiH \rightarrow 2Li_2Mg(NH)_2 + H_2 \quad (5)$$

There was no evidence indicating an interaction between Al and the reactants at this stage. Therefore, taking into account that the equilibrium hydrogen pressure at 200 °C for the Al-doped $Mg(NH_2)_2 + 2LiH$ composite is about the same as for the undoped one, but with an improvement in its dehydrogenation kinetics (Fig. 2), the role of Al seems to be catalytic. However, subsequent hydrogen cycles induced changes in the composite due to the formation of an unknown phase (FTIR band identified at 3232 cm^{-1}), which could be responsible for the decrease in the dehydrogenation rate (Fig. 2) and the increase in the hydrogen equilibrium pressure observed in the second cycle. It was previously showed that the Al generated from decomposition of $3Mg(NH_2)_2 + 2Li_3AlH_6$ inhibited mass transfer between the phases, resulting in low desorption rates and reduced overall reversible capacity [48]. The evidence collected is not enough to clarify the nature and/or composition of this Al-containing phase, and additional investigations are necessary. However, the interactions between the phases clearly modified the thermodynamic stability of the system.

Table 2
Kinetic constants obtained for the LM, LMAl and LMAlCl systems during the first and second desorption cycles at 200 °C.

System	Temperature (°C)	*k* (1/s)	Kinetic Model
LM	200 °C	3.14 *10^{-5} (1st des cycle) 5.49 *10^{-5} (2nd des cycle)	D4
LMAl	200 °C	4.02 *10^{-5} (1st des cycle) 1.03 *10^{-5} (2nd des cycle)	D4
LMAlCl	200 °C	4.52 *10^{-5} (1st des cycle) 7.12 *10^{-6} (2nd des cycle)	D4

For the $AlCl_3$-doped sample, the thermal treatment promoted the interaction between $AlCl_3$ and $Mg(NH_2)_2$, leading to the formation of two cubic phases in the Li-Al-N-H-Cl system. One of these phases was previously identified as $Li_3Al_{3x}(NH_2)_3Cl_{9x}$ (Space Group $I2_13$) [38], which constituted a new amide-chloride compound reported as isostructural with cubic-$Li_4(NH_2)_3Cl$ [36]. The second FCC phase (space group *Fm*-3*m*) displayed structural similarities with an imide-like phase previously formed by milling $AlCl_3$ and $LiNH_2$ or by the dehydrogenation of $Li_3Al_{3x}(NH_2)_3Cl_{9x}$ in the presence of LiH [38]. This last phase showed a FTIR band at 3150 cm^{-1} [38], which is not observed in Fig. 5. In contrast, $LiAl_x(NH_2)Cl_{3x}$ was related with a band at 3245 cm^{-1}, in a similar way to the $Li_3Al_{3x}(NH_2)_3Cl_{9x}$. Consequently, the reaction of as-milled $2LiNH_2 + MgH_2 + 0.09AlCl_3$ during heating under hydrogen pressure can be expressed as follows:

$$Mg(NH_2)_{2(s)} + 2LiH_{(s)} + xAlCl_{3(s)} \text{—} thermal\ treatment \rightarrow 1/6Li_3Al_{3x}(NH_2)_3Cl_{9x(s)} + 1/2LiAl_x(NH_2)Cl_{3x(s)} + 1/2\ MgH_{2(s)} + 1/2\ Mg(NH_2)_{2(s)} + LiH_{(s)} \quad (6)$$

where $LiAl_x(NH_2)Cl_{3x}$ is the imide-like phase, by analogy to similar Li-N-H systems containing LiCl, $MgCl_2$ or $AlCl_3$ [36,38].

The reversibility of the new composite obtained after the thermal treatment (reaction 6) was restricted by two factors: first, the relative amount of LiH with respect to $Mg(NH_2)_2$, $Li_3Al_{3x}(NH_2)_3Cl_{9x}$ and $LiAl_x(NH_2)Cl_{3x}$; and second, the experimental conditions selected in this study (200 °C and 6.0 MPa). In fact, dehydrogenation/rehydrogenation of $Mg(NH_2)_2$ were previously demonstrated via reactions (4) and (5) under similar experimental conditions [17]. In addition, cubic $Li_3Al_{3x}(NH_2)_3Cl_{9x}$ phase showed reversibility at 300 °C and 6.0 MPa of hydrogen [38]. According to previous work [36,38], dehydrogenation of amide-chloride phase could be described by the reaction (7):

$$Li_3Al_{3x}(NH_2)_3Cl_{9x}(s) + 3\ LiH(s) \rightarrow 3\ Li_2Al_x(NH)Cl_{3x}(s) + 3H_2(g) \quad (7)$$

Therefore, the dehydrogenation of $Mg(NH_2)_2$ and $Li_3Al_{3x}(NH_2)_3Cl_{9x}$ according to reactions (4), (5) and (7) is only

partial, due to both the availability of LiH and the experimental conditions applied. Moreover, the fastest dehydrogenation rate observed for the $AlCl_3$-doped sample (Fig. 2) can be associated with the highest hydrogen equilibrium pressure of the resulting $Mg(NH_2)_2$-$Li_3Al_{3x}(NH_2)_3Cl_{9x}$-LiH composite (Fig. 8). The increased kinetic rate noted in the first dehydrogenation step for the $AlCl_3$-doped system is a further evidence of the unique properties of these amide structures improving their hydrogen storage performance by introducing new elements (i.e. Al, Mg), as also predicted by Rijssenbeek et al. [49].

4. Conclusions

Aluminum-compound-doped $2LiNH_2$-MgH_2 composites were prepared by ball milling and heat treatment under 6.0 MPa of hydrogen and their hydrogen storage properties were investigated. Initially, the Al addition to the $2LiNH_2 + MgH_2$ composite improved the dehydrogenation process at 200 °C, apparently due to a catalytic effect. At this stage, no structural modifications due to the reaction between Al and Li-Mg-N-H were detected. A posterior dehydrogenation cycle led to the observation of a new amide phase, which accounted for the increase of the equilibrium hydrogen pressure. Simultaneously, the dehydrogenation rate of the Al-modified sample decreased due to mass transfer constrains. Interestingly, the $AlCl_3$-doped $2LiNH_2 + MgH_2$ sample exhibited the better dehydrogenation rate at 200 °C, which was about three times faster than that of the pristine material. Structural analyses performed by XRPD and FTIR demonstrated that $AlCl_3$ reacted with $LiNH_2$ (during milling and thermal treatment) to form two cubic structures belonging the Li-Al-N-H-Cl system. The formed amide-chloride phases modified both the reaction pathway and the thermodynamic stability of the $AlCl_3$-doped Li-Mg-N-H system. The *in situ* interaction of $AlCl_3$ with $2LiNH_2 + MgH_2$ composite improved the dehydrogenation kinetics without modifying the rate controlling step. However, the formation of amide-chloride phases influenced the reaction pathway. This investigation showed the possibility of improving the dehydrogenation rate and to modify the reaction pathway by anion and/or cation doping.

Acknowledgment

L. F. A. and F. C. G. thank CONICET (the National Council of Scientific and Technological Research) and CNEA (the National Commission of Atomic Energy), ANPCyT (National Promotion Agency of Scientific and technological). F. C. G gratefully acknowledges the financial support from L'Oréal-UNESCO National Award for Women in Science, in collaboration with CONICET (2016). A.S. acknowledges the European Marie Curie Actions (ECOSTORE - Grant Agreement 607040). The activity of N. Senes is supported by a PhD program in a collaborative scheme between the University of Sassari and Cagliari of Italy, which is especially endorsed by Autonomous Regional Administration of Sardinia (RAS). This study has been partially supported by bilateral collaboration Project MINCyT-MAE.

References

[1] J. Tollefson, K.R. Weiss, Nations adopt historic global climate change accord, Nat. News 528 (2015) 315–316.
[2] A. Züttel, A. Borgschulte, L. Schlapbach, Hydrogen as a Future Energy Carrier, first ed., WILEY-VCH, Weinheim, 2007.
[3] M.B. Ley, L.H. Jepsen, Y.-S. Lee, Y.W. Cho, J.M. Bellosta von Colbe, M. Dornheim, M. Rokni, J.O. Jensen, M. Sloth, Y. Filinchuk, J.E. Jørgensen, F. Besenbacher, T.R. Jensen, Complex hydrides for hydrogen storage – new perspectives, Mater. Today 17 (3) (2014) 122–128.
[4] Q. Lai, M. Paskevicius, D.A. Sheppard, C.E. Buckley, A.W. Thornton, M.R. Hill, Q. Gu, J. Mao, Z. Huang, H.K. Liu, Z. Guo, A. Banerjee, S. Chakraborty, R. Ahuja, K.-F. Aguey-Zinsou, Hydrogen storage materials for mobile and stationary applications: current state of the art, ChemSusChem 8 (17) (2015) 2789–2825.
[5] Y. Liu, Y. Yang, M. Gao, H. Pan, Tailoring thermodynamics and kinetics for hydrogen storage in complex hydrides towards applications, Chem. Rec. 16 (1) (2016) 189–204.
[6] S. Orimo, Y. Nakamori, J.R. Eliseo, A. Züttel, C.M. Jensen, Complex hydrides for hydrogen storage, Chem. Rev. 107 (2007) 4111–4132.
[7] M. Paskevicius, L.H. Jepsen, P. Schouwink, R. Černý, D.B. Ravnsbæk, Y. Filinchuk, M. Dornheim, F. Besenbacher, T.R. Jensen, Metal borohydrides and derivatives - synthesis, structure and properties, Chem. Soc. Rev. 46 (5) (2017) 1565–1634.
[8] T. He, P. Pachfule, H. Wu, Q. Xu, P. Chen, Hydrogen carriers, Nat. Rev. Mater. 1 (2016) 16059.
[9] P. Chen, Z. Xiong, J. Luo, J. Lin, L.T. Tan, Interaction of hydrogen with metal nitrides and imides, Nature 420 – 421 (2002) 302–304.
[10] W. Luo, ($LiNH_2$-MgH_2): a viable hydrogen storage system, J. Alloys Compd. 381 (1–2) (2004) 284–287.
[11] Z.T. Xiong, G.T. Wu, H.J. Hu, P. Chen, Ternary imides for hydrogen storage, Adv. Mater. 16 (2004) 1522–1525.
[12] W. Luo, E. Rönnebro, Towards a viable hydrogen storage system for transportation application, J. Alloys Compd. 404 (2005) 392–395.
[13] W. Luo, V. Stavila, L.E. Klebanoff, New insights into the mechanism of activation and hydrogen absorption of ($2LiNH_2$-MgH_2), Int. J. Hydrogen Energy 37 (8) (2012) 6646–6652.
[14] Z. Xiong, J. Hu, G. Wu, P. Chen, W. Luo, K. Gross, J. Wang, Thermodynamic and kinetic investigations of the hydrogen storage in the Li-Mg-N-H system, J. Alloys Compd. 398 (1–2) (2005) 235–239.
[15] H. Wang, G. Wu, H. Cao, C. Pistidda, A.L. Chaudhary, S. Garroni, M. Dornheim, P. Chen, Near ambient condition hydrogen storage in a synergized tri component hydride system, Adv. Energy Mater. 7 (13) (2017), 1602456.
[16] H. Cao, G. Wu, Y. Zhang, Z. Xiong, J. Qiu, P. Chen, Effective thermodynamic alteration to $Mg(NH_2)_2$ –LiH system: achieving near ambient-temperature hydrogen storage, J. Mater. Chem. A 2 (38) (2014) 15816–15822.
[17] G. Amica, F. Cova, P. Arneodo Larochette, F.C. Gennari, Effective participation of $Li_4(NH_2)_3BH_4$ in the dehydrogenation pathway of the $Mg(NH_2)_2$-2LiH composite, Phys. Chem. Chem. Phys. 18 (27) (2016) 17997–18005.
[18] W.I.F. David, M.O. Jones, D.H. Gregory, M. Jewell, S.R. Johnson, A. Walton, P.P. Edwards, A mechanism for non-stoichiometry in the lithium amide/lithium imide hydrogen storage reaction, J. Am. Chem. Soc. 129 (6) (2007) 1594–1601.
[19] F. Torre, A. Valentoni, C. Milanese, C. Pistidda, A. Marini, M. Dornheim, S. Enzo, G. Mulas, S. Garroni, Kinetic improvement on the CaH_2-catalyzed $Mg(NH_2)_2$ + 2LiH system, J. Alloys Compd. 645 (2015) S284–S287.
[20] J. Hayes, A. Goudy, Thermodynamics, kinetics and modeling studies of KH-RbH- and CsH-doped $2LiNH_2/MgH_2$ hydrogen storage systems, Int. J. Hydrogen Energy 40 (36) (2015) 12336–12342.
[21] B. Li, Y. Liu, C. Li, M. Gao, H. Pan, In situ formation of lithium fast-ion conductors and improved hydrogen desorption properties of the $LiNH_2$–MgH_2 system with the addition of lithium halides, J. Mater. Chem. A 2 (9) (2014) 3155–3162.
[22] H. Cao, H. Wang, T. He, G. Wu, Z. Xiong, J. Qiu, P. Chen, Improved kinetics of the $Mg(NH_2)_2$ –2LiH system by addition of lithium halides, RSC Adv. 4 (61) (2014) 32555–32561.
[23] J. Wang, T. Liu, G. Wu, W. Li, Y. Liu, C.M. Araújo, H.R.H. Scheicher, A. Blomqvist, R. Ahuja, Z. Xiong, P. Yang, M. Gao, Hongge Pan, P. Chen, Potassium-modified $Mg(NH_2)_2$/2LiH system for hydrogen storage, Angew. Chem. Int. Ed. 48 (32) (2009) 5828–5832.
[24] Y. Liu, C. Li, B. Li, M. Gao, H. Pan, Metathesis reaction-induced significant improvement in hydrogen storage properties of the KF-added Mg $(NH_2)_2$ – 2LiH system, J. Phys. Chem. C 117 (2013) 866–875.
[25] H. Cao, H. Wang, C. Pistidda, C. Milanese, W. Zhang, A. Chaudhary, A. Santoru, S. Garroni, J. Bednarcik, H. Liermann, P.T. Klassen, M. Dornheim, The effect of $Sr(OH)_2$ on the hydrogen storage properties of the $Mg(NH_2)_2$–2LiH system, Phys. Chem. Chem. Phys. 19 (2017) 8457–8464.
[26] S. Nayebossadri, Kinetic rate-limiting steps in dehydrogenation of Li-N-H and Li-Mg-N-H systems - effects of elemental Si and Al, Int. J. Hydrogen Energy 36 (14) (2011) 8335–8343.
[27] C. Li, Y. Liu, Y. Pang, Y. Gu, M. Gao, H. Pan, Compositional effects on the hydrogen storage properties of $Mg(NH_2)_2$-2LiH-xKH and the activity of KH during dehydrogenation reactions, Dalton Trans. 43 (2014) 2369–2377.
[28] C. Li, Y. Liu, Y. Yang, M. Gao, H. Pan, High-temperature failure behavior and mechanism of K-based additives in Li–Mg–N–H hydrogen storage systems, J. Mater. Chem. A 2 (2014) 7345–7353.
[29] Y. Liu, Y. Yang, X. Zhang, Y. Li, M. Gao, H. Pan, Insights into the dehydrogenation reaction process of a K-containing $Mg(NH_2)_2$–2LiH system, Dalton Trans. 44 (2015) 18012–18018.
[30] J. Zhang, Y. Liu, X. Zhang, Y. Yang, Q. Zhang, T. Jin, Y. Wang, M. Gao, L. Sun, H. Pan, Synthesis of CsH and its effect on the hydrogen storage properties of the $Mg(NH_2)_2$-2LiH system, Int. J. Hydrogen Energy 41 (2016) 11264–11274.
[31] T. Durojaiye, J. Hayes, A. Goudy, A. Potassium, Rubidium and cesium hydrides as dehydrogenation catalysts for the lithium amide/magnesium hydride system, Int. J. Hydrogen Energy 40 (2015) 2266–2273.
[32] N. Gamba, P. Arneodo Larochette, F.C. Gennari, Effect of LiCl presence on the hydrogen storage performance of the $Mg(NH_2)_2$–2LiH composite, RSC Adv. 5

(2015) 68542–68550.
[33] R. Bill, D. Reed, D. Book, P. Anderson, Effect of the calcium halides, $CaCl_2$ and $CaBr_2$, on hydrogen desorption in the Li-Mg-N-H system, J. Alloys Compd. 645 (2015) 96–99.
[34] G. Amica, S. Enzo, P. Arneodo Larochette, F.C. Gennari, Improvements in the hydrogen storage properties of the $Mg(NH_2)_2$-LiH composite by KOH addition, Phys. Chem. Chem. Phys. (2018), https://doi.org/10.1039/C8CP02347F.
[35] S. Garroni, A. Santoru, H. Cao, M. Dornheim, T. Klassen, C. Milanese, F. Gennari, C. Pistidda, Recent progress and new perspectives on metal amide and imide systems for solid-state hydrogen storage, Energies 11 (2018) 1027, https://doi.org/10.3390/en11051027.
[36] P.A. Anderson, P.A. Chater, D.R. Hewett, P.R. Slater, Hydrogen storage and ionic mobility in amide-halide systems, Faraday Discuss 151 (2011) 271–295.
[37] L. FernandezAlbanesi, S. Garroni, P. Arneodo Larochette, P. Nolis, G. Mulas, S. Enzo, M. Dolors Baro, F.C. Gennari, Role of aluminum chloride on the reversible hydrogen storage properties of the Li-N-H system, Int. J. Hydrogen Energy 40 (2015) 13506–13517.
[38] L. Fernández Albanesi, S. Garroni, S. Enzo, F.C. Gennari, New amide–chloride phases in the Li–Al–N–H–Cl system: formation and hydrogen storage behaviour, Dalton Trans. 45 (13) (2016) 5808–5814.
[39] L. Fernández Albanesi, P. Arneodo Larochette, F.C. Gennari, Destabilization of the $LiNH_2$-LiH hydrogen storage system by aluminium incorporation, Int. J. Hydrogen Energy 38 (28) (2013) 12325–12334.
[40] L. Lutterotti, P. Scardi, Simultaneous structure and size-strain refinement by the Rietveld method, J. Appl. Crystallogr. 23 (1990) 246–252.
[41] L.H. Jepsen, D.B. Ravnsbæk, C. Grundlach, F. Besenbacher, J. Skibsted, T.R. Jensen, A novel intermediate in the $LiAlH_4$-$LiNH_2$ hydrogen storage system, Dalton Trans. 43 (2014) 3095–3103.
[42] H. Cao, Y. Zhang, J. Wang, Z. Xiong, G. Wu, J. Qiu, P. Chen, Effects of Al-based additives on the hydrogen storage performance of the $Mg(NH_2)_2$-2LiH system, Dalton Trans. 42 (2013) 5524–5531.
[43] J.S. Sharp, G.W. Brindley, B.N. Narahari Achar, Numerical data for some commonly used solid stare reaction equations, J. Am. Ceram. Soc. 49 (1966) 379–382.
[44] J. Beretka, Kinetic analysis of solid-stare reactions between powdered reactants, J. Am. Ceram. Soc. 67 (1984) 615–620.
[45] G. Barkhordarian, T. Klassen, R. Bormann, Kinetic investigation of the effect of milling time on the hydrogen sorption reaction of magnesium catalyzed with different Nb_2O_5 contents, J. Alloys Compd. 407 (2006) 249–255.
[46] S. Vyazovkin, A.K. Burnham, J.M. Criado, L.A. Pérez-Maqueda, C. Popescu, N. Sbirrazzuoli, ICTAC Kinetics Committee recommendations for performing kinetic computations on thermal analysis data, Thermochim. Acta 520 (2011) 1–19.
[47] J. Hu, Y. Liu, G. Wu, Z. Xiong, P. Chen, Structural and compositional changes during hydrogenation/dehydrogenation of the Li–Mg–N–H system, J. Phys. Chem. C111 (2007) 18439–18443.
[48] D. Liu, A. Sudik, J. Yang, P. Ferro, C. Wolverton, Hydrogen storage properties of $3Mg(NH_2)_2$-$2Li_3AlH_6$, J. Phys. Chem. C 116 (2012) 1485–1492.
[49] J. Rijssenbeek, Y. Gao, J. Hanson, Q. Huang, C. Jones, B. Toby, Crystal structure determination and reaction pathway of amide–hydride mixtures, J. Alloys Compd. 454 (2008) 233–244.